

Three-dimensional data of wirecut surface scans under the confocal microscope (110 character maximum, inc. spaces)

Yuhang Lin^{1,2,*}, Heike Hofmann^{2,3}, Curtis Mosher⁴, Eden Amin⁵, Jeff Salyards², and Alicia Carriquiry^{1,2}

¹Iowa State University, Department of Statistics, Ames, IA, 50011, USA

²Iowa State University, Center for Statistics and Applications in Forensic Evidence, Ames, IA, 50011, USA

³University of Nebraska-Lincoln, Department of Statistics, Lincoln, NE, 68583, USA

⁴Iowa State University, Roy J Carver High Resolution Microscopy Facility, Ames, IA, 50011, USA

⁵University of Central Oklahoma, Forensic Science Institute, Edmond, OK, 73034, USA

*corresponding author(s): Yuhang Lin (yhlin@iastate.edu)

ABSTRACT

Update later: max of 170 words: describe the study, the assay(s) performed, resulting data, and reuse potential

Wire cut data is important in forensic investigations but lacks a systematic way of analyzing the data. We created a dataset of 120 scans of aluminum wire cut in $\times 3p$ format, using 5 wire cutters and 3 locations along the 4 blades, with 2 replicates for each combination. A systematic pipeline with multiple analysis plots was developed to analyze the data and draw conclusions based on numerical measures.

Background & Summary

An important aspect of forensic analysis involves investigating marks left at crime scenes. Forensic examiners focus particularly on identifying the origin of these marks, a process known as the Source Identification Problem in Forensic Science¹ citation?. The forensic science community generally distinguishes between the **specific source problem**, where the examiner seeks to determine whether a mark was left by a particular tool, and the **common source problem**, which focuses on whether two marks were left by the same tool. Currently, accepted practice in both of these two problems relies on visual inspection of the items under a comparison microscope. The results, according to the Theory of Identification² developed by the Association of Firearm and Toolmark Examiners (AFTE), are categorized by examiner into three types: *identification*, where the marks are believed to have been made by the same source; *elimination*, where the marks are believed to have been made by different tools; and *inconclusive*, where similarities or dissimilarities between the marks are insufficient to allow either an identification or an elimination. However, this assessment is inherently subjective, which has led to criticism from reports by the National Research Council (NRC)³ and the President's Council of Advisors on Science and Technology (PCAST)⁴ for lacking quantifiable measures of objectivity and the absence of error rates. Such limitations highlight the need for empirical datasets with known ground truth to validate conclusions. Addressing this gap requires a structured approach that not only evaluates examiner performance but also considers case-specific evidence in a measurable way. To bridge this gap, it is necessary to establish a framework that integrates both empirical validation of examiner performance and measurable analysis of case-specific evidence. A crucial aspect of this framework is recognizing different methodological perspectives in forensic science.

In this context, Biedermann⁵ differentiates between internal and external perspectives in the forensic literature. The external perspective only allows general statements based on (black-box) studies relating examiners' conclusions to ground truth without considering any evidence of a particular case. To allow an internal perspective, there is a need to quantitatively capture the basis for an evaluation based on specific evidence. To transition toward an internal perspective, similarity comparisons are needed. However, no publicly available dataset currently exists for wirecut marks. The closest work is by Baiker et al.⁶, which focuses on screwdriver toolmarks, not wire cutters. Thus, there is an urgent need to collect and analyze public datasets specific to wirecut marks.

Understanding the characteristics of toolmarks left by wire cutters is essential. When a bladed tool cuts a wire, it leaves striations on the cut surface, as shown in Figure 1. These striations serve as evidence to assess the similarity. There have been cases where the evidence and testimony on wire cut evidence played a crucial role in the criminal investigation and conviction



Figure 1. Microscopic close-up of striations left by a blade on the cut end of a wire.

of a defendant. However, forensic analysis of these evidence lacks a standardized quantitative approach, except for visual comparisons.

A growing of research has sought to develop quantitative methods for analyzing forensic toolmarks, particularly those created by different types of tools. Prior studies on striated toolmarks provide insights into key comparison factors, including angle of attack⁶, rotational axis⁷, and cutting direction⁸. Foundational research in forensic toolmarks has emphasized dataset collection and computational analysis. Ma et al.⁹ and Zheng et al.¹⁰ focused on collecting and distributing datasets for bullet and toolmark analysis for this purpose. Chu et al.¹¹ and Vorburger et al.¹² demonstrated numerical methods for improving accuracy and consistency. Hare et al.¹³ and Ju et al.¹⁴ developed similarity quantification techniques, but alignment remains a major challenge.

In this study, we build on these methodologies to provide a publicly available dataset of wirecut scans, develop a systematic pipeline to analyze the data quantitatively, and introduce numerical measures for similarity assessment beyond visual inspection. The dataset includes multiple types of files, as summarized in Table 1.

To ensure full reproducibility, we describe each step in detail, including how we collected and processed the wirecut samples in [Cutting Wires](#) hyperlink location incorrect for unnumbered sections it seems that the hyperlinks make sure that the section is on the page, profile extraction from scanned surfaces in [Extract Profiles](#) how we extract profiles from the scans, filtering signals from profiles in [Filtered Signals](#), and alignment methodologies using the cross-correlation function (CCF) in [Align Signals](#). The details regarding dataset hosting are discussed in [Data Records](#). A technical validation of consistency of assumptions and conclusions is provided in [Technical Validation](#). [Usage Notes](#) includes open-source code for dataset generation and analysis, as discussed in [Methods](#) and [Technical Validation](#). Finally, in [Code availability](#), we discuss access to our code for reproducibility and future research. We anticipate that this dataset and analysis pipeline will serve as a foundation for forensic practitioners and be extended to real-world crime scene investigations involving wirecut evidence.

63 Methods

64 In this study, we use aluminium wire [more details: thickness, brand?](#) to create cuts. The physical property of aluminum wire
65 makes it an excellent candidate for keeping marks while being relatively easy to bend and non-toxic, i.e. with a hardness of
66 XXX aluminium is soft enough that tools leave marks, but hard enough to not be affected by handling cut materials under the
67 microscope.

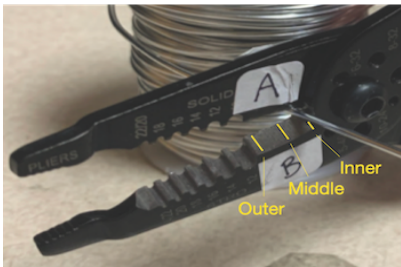
68 [XXX look up the hardness value of aluminium, copper and lead.](#) In real casework, aluminium wires are not seen as often
69 as lead or copper. We avoided using lead in the laboratory setting, because of its toxicity.

70 Cutting Wires

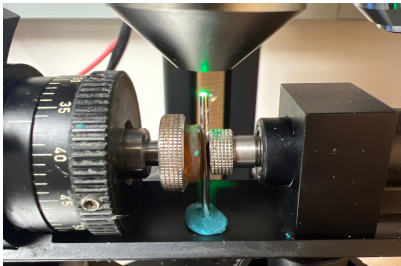
71 The aluminum wire used was 16 Gauge/1.5 mm, anodized. In order to cut the wire, 4-inch pieces were unspooled and cut
72 using Kaiweets wire cutters, model KWS-105, as shown in Figure 2a, for 1 blade location, either inner, middle, or outer, which

Table 1. Structure of available data and files.

	Description	Section
Raw data		
scans/	folder containing 120 topographic 3d scans	Cutting Wires
meta.csv	corresponding to 30 aluminum wire cuts (x3p format) meta information for each cut with tool, blade, and location information (CSV format)	Cutting Wires
Manual derivatives		
profiles/	folder of files with manually extracted profiles (CSV format)	Extract Profiles
Computational derivatives in folder 'data-derived/'		
wire-signals	signals processed from corresponding profile (zipped CSV format)	Filtered Signals
wire_pairwise_ccf	CCF values of all pairwise aligned signals (zipped CSV format)	Align Signals
Image files		
pngs/	folder containing pictures of 3d scans of wire cuts (PNG format)	Cutting Wires
profile-images/	folder containing pictures of profile extracted from wire cuts (PNG format)	Extract Profiles
Visual Inventory in folder 'assessment/analysis-manual/'		
processing-wires	display of pairwise aligned signals from the same sources (HTML format)	Align Signals



(a)

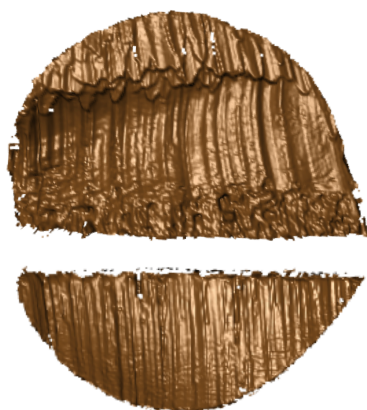


(b)

Blade A



Blade C



Blade B

(c)

Figure 2. (a) A Kaiweets wire cutter of model KWS-105 was used to cut the wire, with inner, middle and outer locations marked. (b) A confocal microscope was used to scan the wire surfaces. (c) After separating 2 tent structures by the connecting position, we obtained 4 samples - 2 samples from blade A and B, and others from blade C and D. width and height are tuned manually | full requirements see <https://www.nature.com/sdata/publish/submission-guidelines#figures>

gives us 1 replicate. Each piece was then cut into half to create 2-inch pieces for each side, AB and CD, with a sharpie line marking the cut ends, giving us 4 samples. Then, we use the standard scanning protocols for the confocal microscope, shown in Figure Figure 2b, to scan the wire tip surfaces. The scanned surfaces are saved in a resolution of $0.645\mu m \times 0.645\mu m$ per square pixel in an x3p file format. Here, we are showing AB and CD sides in Figure 2c, with the back of A being C and the back of B being D. Both AB and CD sides form tent structures on the tips of the wire, and we separate each side of the tent into 2 pieces along the bending position, resulting in 8 scans. We repeated this process for all 3 locations along the blade and 5 wire cutters, with 2 replicates for each tool-edge-location combination, resulting in 120 scans. Each piece was labeled with the naming conventions, T(ool) 1/2/3/4/5 (Edge) A/B/C/D W(ire) - L(ocation) I(nner)/M(iddle)/O(uter) - R(epetition) 1/2, with T1AW-LI-R1 being the piece cut by tool 1 on the A edge at the inner location for the first repetition.

Extract Profiles

Numerical comparisons between 2 replicates cannot be done directly on the x3p files. We need to extract representative functions from the scans first. A representative function with the most information is considered as a signal for one scan, which is used later for comparison. To obtain this function, we first need a profile of the scan, which is a sequence of values along a user-drawn line on the surface. The profile captures most features of the scan and be orthogonal to the striation marks of the scan, which are formed by the ups and downs of grooves. So, we draw the line across the wide region of the scan to maximize the feature captured, as shown in dark blue in Figure 3a. We then investigate the values under this profile line. The profile function along the line is plotted in Figure 3b.

Filtered Signals

With the profile extracted, we then obtain the signal. Two Gaussian filters, as discussed in Cleveland et al.¹⁵, are applied to these resulting profiles. In particular, we first used a large low-pass filter with bandwidths of 400 microns to remove the large trend, as it overwhelms the signals, and then used a small high-pass filter of 40 microns to average across noise and remove spikes, as shown in Figure 3c. Finally, the extreme tail values are removed.

Align Signals

Signals extracted from different scans are put together for comparison, and we maximize the cross-correlation function (CCF) values between the signals to find the best alignment numerically. For example, we compare T1AW-LI-R1 to T1AW-LI-R2, T1CW-LI-R1 to T1CW-LI-R2, and so on. That is comparing each row in Figure 4. We know that signals from two replicates

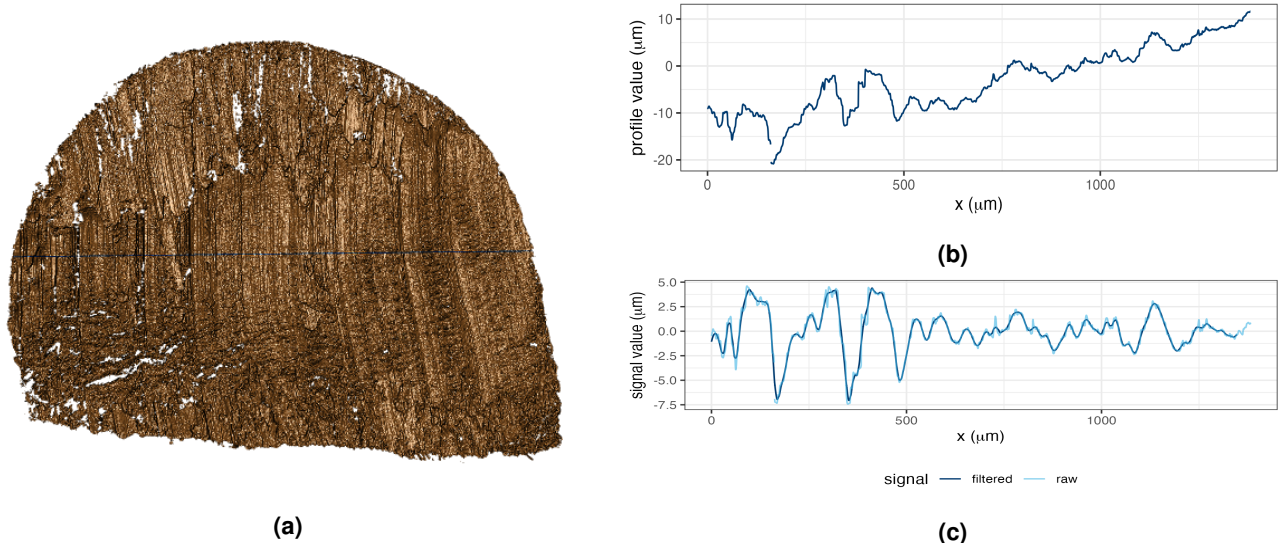


Figure 3. (a) A profile line in dark blue was drawn across the striations of the scan. (b) The profile function extracted along the profile line in (a). (c) The raw signal in light blue is obtained by using the low-pass filter on the profile function in (b) and the filtered signal is obtained by using the high-pass filter on the raw signal.

with the same tool-edge-location combination yield similar signals as in the first and second columns of Figure 5, which results in alignments of massive overlapping and high CCF values close to 1. The alignments and values we got in the rightmost column of Figure 5 fulfill our expectations.

102 Data Records

¹⁰³ The complete dataset is available on the ISU DataShare repository at <https://iastate.figshare.com/>, which is public and open
¹⁰⁴ access for every interested researcher. The structure of the dataset is described before in Table 1.

105 Technical Validation

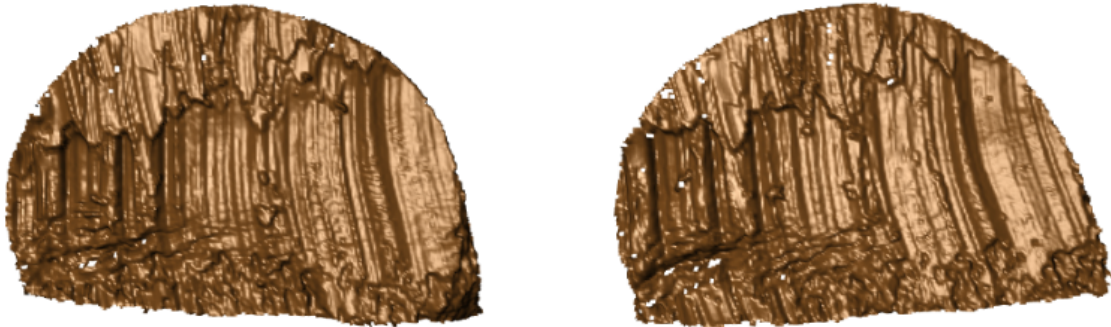
106 For the data collection process, two team members did the cutting and labeling together, then one person did the scanning and
107 named according to the naming convention introduced in [Cutting Wires](#). The scanning was done in a specific order to ensure
108 consistency across all scans. The data was saved in a consistent format to ensure easy of access for analysis. A third person
109 then checked the data to ensure that the data was consistent in naming and accurate.

While the difference between the order of profiles extracted and the person who extracted the profile remains another huge area for research, we leave that for further discussion and only include the difference between staging and acquisitions in this technical validation process. We examined how the data acquisition process influences variability in the final scans saved in $\times 3p$. For this, we arbitrarily selected scans from tool 2 at location middle. First, we obtained the average CCF between replicates (replicate 1 and replicate 2) through pairwise comparison. Then, we rescanned replicate 2 under the confocal microscope, introducing a new staging labeled as S. Staging 1 for replicate 2 is omitted in the label, resulting in R2(-S1). For all four edges of tool 2 at location middle, we created three different stagings: R2, R2-S2, and R2-S3, and computed the average CCF between stagings using pairwise comparison.

Within each staging, we further examined the effect of different acquisitions by keeping the scans on the confocal microscope under varying lighting conditions, introducing a new acquisition label as A. For edge A at staging 3, we performed four acquisitions in total, omitting the first one in the label again, resulting in R2-S3(-A1). For the other three edges, we conducted two acquisitions in staging 3, denoted as R2-S3 and R2-S3-A2. The average CCF between acquisitions was then obtained through pairwise comparison.

With this setup, we expect increasing consistency in the CCF from replicate to staging to acquisition, as conditions become progressively more stable. Consequently, variability should decrease along this sequence. We also computed the differences between replicate, staging, and acquisition, expecting smaller differences between acquisition and staging compared to those between staging and replicate. We can visualize the results as scatter plots, as shown in Figure 6. The interval within 2 SD is also shown. There is an increase in the average as shown as orange bar and a decrease in standard deviation (SD) as shown

Edge A



Edge C



Edge B



Edge D



Figure 4. Scans from different sides of tool 1 at the inner location.

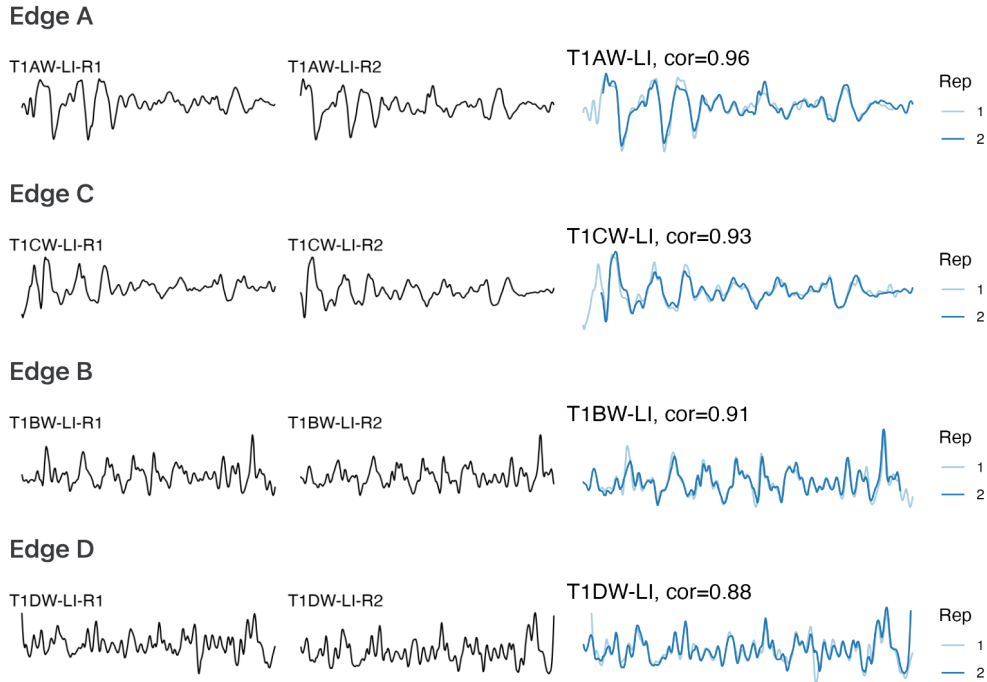


Figure 5. The first and second columns show the signals extracted from Figure 4, and the third column shows the alignments and CCF values between pairs of signals.

Table 2. Comparison of CCF across different settings.

Edge	Replicate		Staging			Acquisition		
	Avg CCF	SD	Avg CCF	SD	(Staging - Replicate)	Avg CCF	SD	(Acquisition - Staging)
A	0.818	0.015	0.961	0.012	0.143	0.992	0.003	0.031
B	0.879	0.031	0.922	0.042	0.043	0.939	NA	0.017
C	0.841	0.022	0.952	0.021	0.111	0.959	NA	0.007
D	0.797	0.011	0.966	0.017	0.169	0.986	NA	0.020

in the interval width in the plot. The detailed numeric results, together with standard deviation and differences in averages, shown in Table 2, confirm our expectations.

For the validation of the scans and their processing, we investigate the correlation scores of pairwise aligned signals. Large scores between signals are indicative of being made by the same tool. As shown previously in Figure 5 in [Align Signals](#), we expect a high correlation score between signals from scans of wires cut with the same tool. For signals from scans of wires cut with a different tool, we expect a low correlation score. For example, we have two scans from different tools, T1AW-LI-R1 and T2AW-LI-R1, as shown in Figure 7a and Figure 7b. The alignment is shown in Figure 7c with a 0.2 CCF value, which is low, as expected.

We also put resulting CCFs for all pairwise comparisons in the boxplot, together with the receiver operating characteristic (ROC) curve, as in Figure 8 and Figure 9. The CCF values for the same sources are close to 1, while the CCF values for different sources are much lower than expected. This is consistent with our expectations and validates our data processing pipeline.

Usage Notes

The R package `x3ptools`¹⁶ available from CRAN supports working with files in `x3p` format. The sample scripts in R for processing scans from `x3p` format to their signal and alignment are available on GitHub [heike/wirecuts-data](#) in the assessment/code folder, as described in Table 3.

We already conduct pairwise comparisons and visualize some of the comparison results in [Align Signals](#) and [Technical](#)

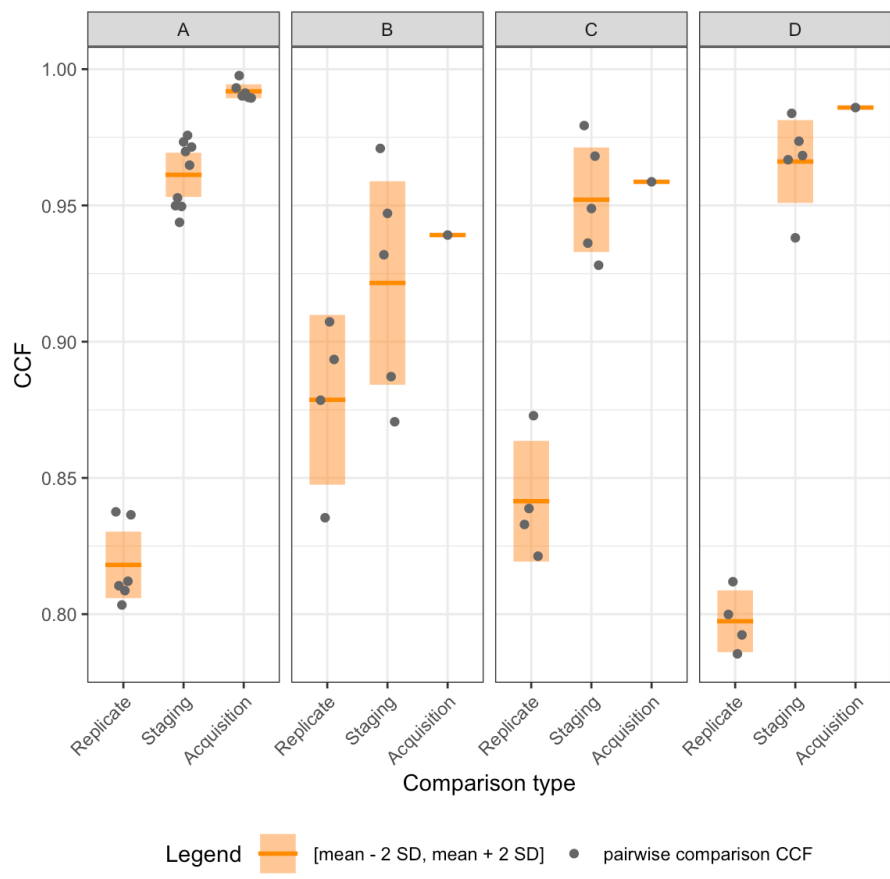


Figure 6

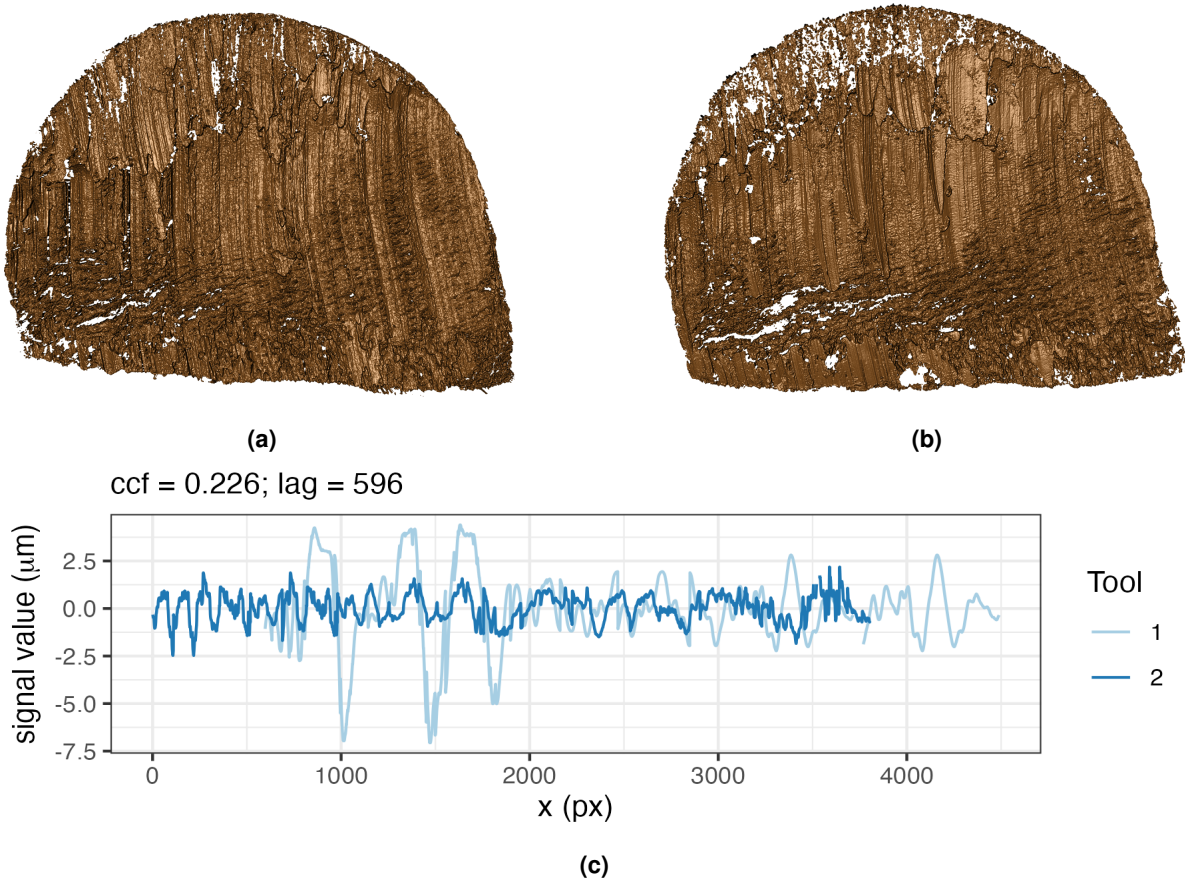


Figure 7. (a) Scan T1AW-LI-R1 cut by tool 1. (b) Scan T2AW-LI-R1 cut by tool 2. (c) Alignment of signals from T1AW-LI-R1 and T2AW-LI-R1.

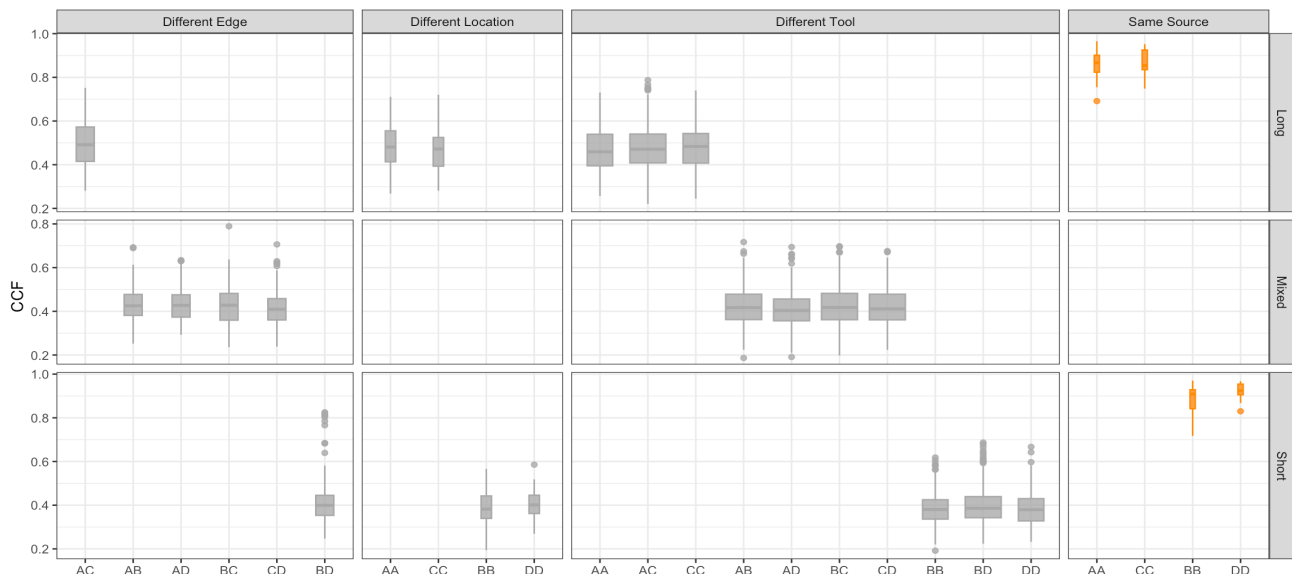


Figure 8. The boxplot shows that signals from the same sources have higher CCFs than those from different sources.

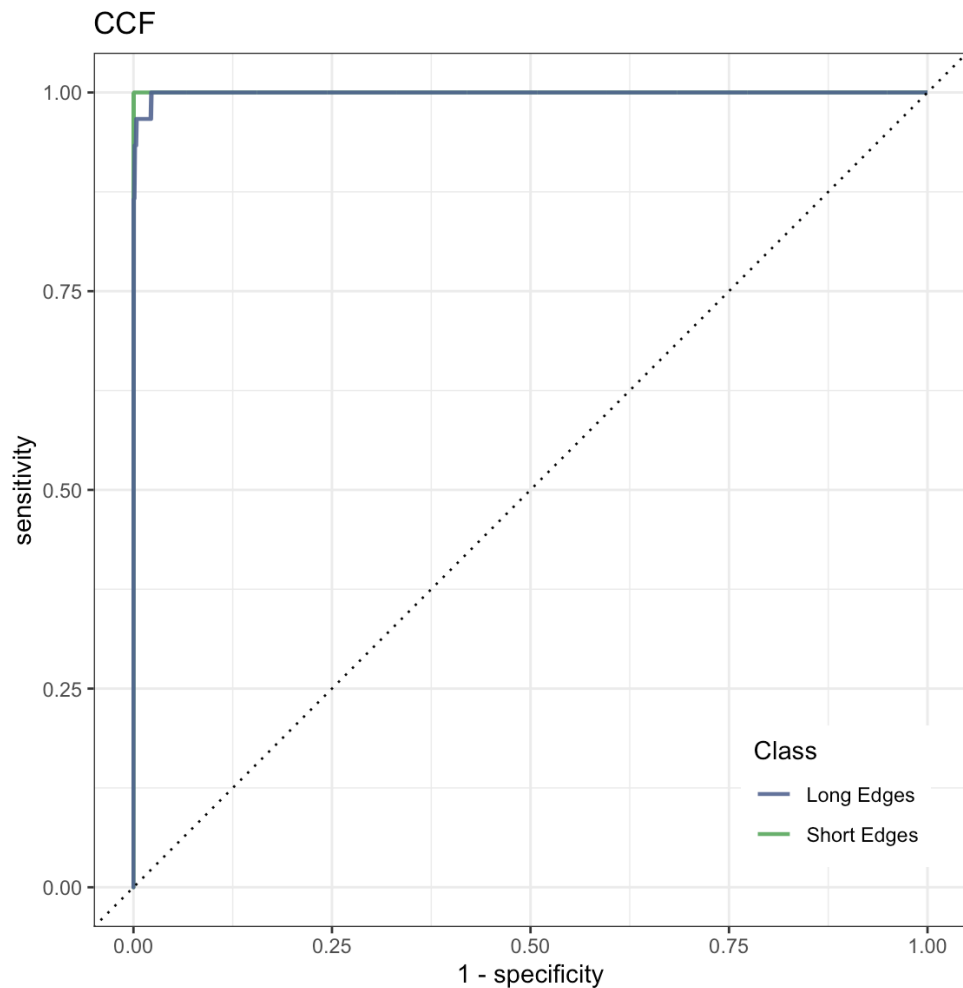


Figure 9. The ROC curve is bending very close to the upper left corner, which means excellent in classification and drawing conclusions.

Table 3. Overview of available codes.

	Description	Section
Inspect raw scans		
1-create_pngs_from_x3p.R	obtain images of x3ps in scans /	Cutting Wires
Extract profiles		
2-create_profiles_from_x3p.R	manually extract profiles from each scan	Extract Profiles
3-create-single-profile-file.R	create meta profile information	Extract Profiles
Derive signals		
4-create_signals_from_profiles.R	derive signals from each profile	Filtered Signals
Align signals		
5-create-images.R	create images for pairwise alignment	Align Signals
6-align-pairwise.R	compute pairwise alignment CCF values	Align Signals
7-all-comparison-results.R	visualize comparison results	Align Signals

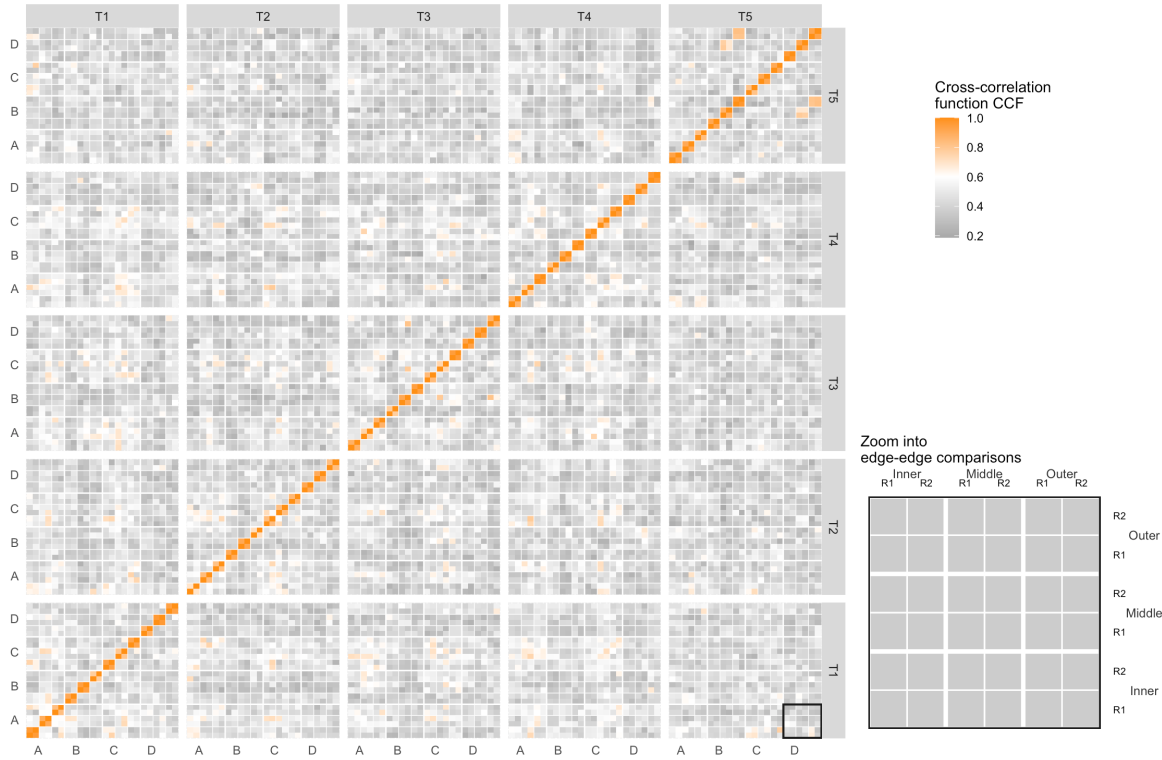


Figure 10. The tilemap shows signals from the same source have CCFs close to 1.

145 **Validation**, and other analysis plots as well.

146 Suppose we put the CCF values in a tilemap with different tools, locations and edge combinations. In that case, we expect
 147 only the diagonal to have high CCF values, close to 1 and marked as orange in the tilemap, as the diagonal represents the
 148 same source, and the rest of the matrix to have low CCF values, close to 0 and marked as gray. In Figure 10, the behavior is
 149 consistent with our expectation overall, except for some rare cases with tool 5 edge D. The density plot in Figure 11 shows the
 150 distribution of the CCF values with the same sources and different sources. The overlapping points between the tails of these
 151 two distributions to be a rough threshold.

152 Furthermore, the ROC curve in Figure 9 shows the sensitivity / true positive rate against the false positive rate (FPR) (1 -
 153 specificity). The curve is very close to the upper left corner, which is excellent for classification and drawing conclusions. It
 154 gives us a true threshold of 0.589 to control the FPR to be less than 0.05 with a false negative rate (FNR) to be 0, (false positive
 155 rate (FPR) / false discovery rate (FDR) -> define the H0 or call it false identification rate (FIR)???, and 0.658 to control the
 156 FPR to be less than 0.01, with FNR to be 0.02.

157 **Code availability**

158 We made available all codes we used for inspecting raw scans, extracting profiles, deriving signals, aligning signals, and visualizing
 159 comparison results discussed in **Methods** and **Technical Validation**, as described in Table 3. All results are reproducible
 160 using these codes provided.

161 **References**

- 162 1. Lindley, D. V. A Problem in Forensic Science. *Biometrika* **64**, 207, [10.2307/2335686](https://doi.org/10.2307/2335686) (1977). [2335686](#).
- 163 2. AFTE. The association of firearm and tool mark examiners: Theory of identification as it relates to toolmarks. *AFTE J.* **30**, 86–88 (1998).
- 164 3. NRC. *National Research Council: Strengthening Forensic Science in the United States: A Path Forward* (National Academies Press, 2009).

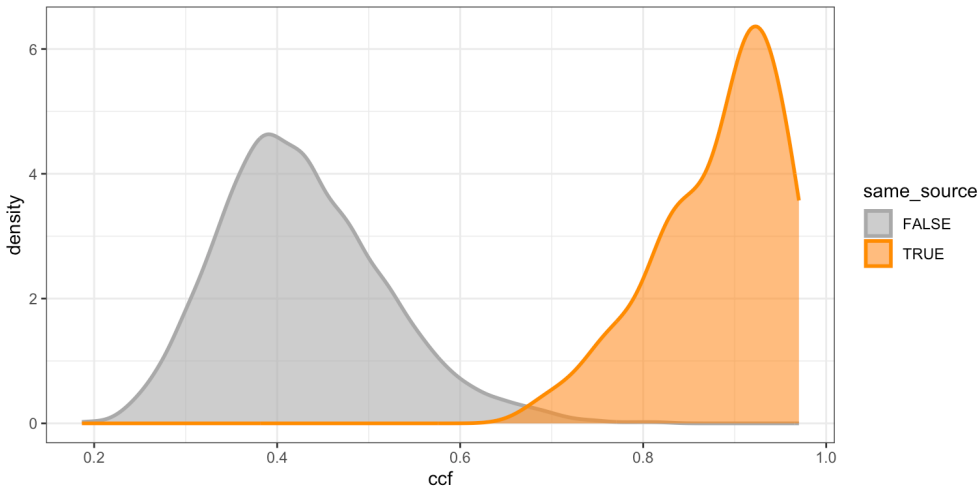


Figure 11. The density plot shows tails of distributions overlap, which to be used as a rough threshold for drawing conclusions.

- 167 4. President's Council of Advisors on Science and Technology. *President's Council of Advisors on Science and Technology: Forensic Science in Criminal Courts: Ensuring Scientific Validity of Feature-Comparison Methods* (Executive Office of the President of the United States, President's Council, Washington, D.C., 2016).
- 168
- 169
- 170 5. Biedermann, A. The strange persistence of (source) “identification” claims in forensic literature through descriptivism, diagnosticism and machinism. *Forensic Sci. Int. Synerg.* **4**, 100222, [10.1016/j.fsisyn.2022.100222](https://doi.org/10.1016/j.fsisyn.2022.100222) (2022).
- 171
- 172 6. Baiker, M., Pieterman, R. & Zoon, P. Toolmark variability and quality depending on the fundamental parameters: Angle of attack, toolmark depth and substrate material. *Forensic Sci. Int.* **251**, 40–49, [10.1016/j.forsciint.2015.03.003](https://doi.org/10.1016/j.forsciint.2015.03.003) (2015).
- 173
- 174 7. Garcia, D. L., Pieterman, R. & Baiker, M. Influence of the axial rotation angle on tool mark striations. *Forensic Sci. Int.* **279**, 203–218, [10.1016/j.forsciint.2017.08.021](https://doi.org/10.1016/j.forsciint.2017.08.021) (2017).
- 175
- 176 8. Cuellar, M., Gao, S. & Hofmann, H. An algorithm for forensic toolmark comparisons. *Forensic Sci. Int. Synerg.* **9**, 100543, [10.1016/j.fsisyn.2024.100543](https://doi.org/10.1016/j.fsisyn.2024.100543) (2024).
- 177
- 178 9. Ma, L. *et al.* NIST Bullet Signature Measurement System for RM (Reference Material) 8240 Standard Bullets. *J. Forensic Sci.* **49**, 1–11, [10.1520/JFS2003384](https://doi.org/10.1520/JFS2003384) (2004).
- 179
- 180 10. Zheng, X. A., Soons, J. A. & Thompson, R. M. NIST Ballistics Toolmark Research Database | NIST (2016).
- 181
- 182 11. Chu, W., Thompson, R. M., Song, J. & Vorburger, T. V. Automatic identification of bullet signatures based on consecutive matching striae (CMS) criteria. *Forensic Sci. Int.* **231**, 137–141, [10/gn65cz](https://doi.org/10/gn65cz) (2013).
- 183
- 184 12. Vorburger, T. *et al.* Applications of cross-correlation functions. *Wear* **271**, 529–533, [10.1016/j.wear.2010.03.030](https://doi.org/10.1016/j.wear.2010.03.030) (2011).
- 185
- 186 13. Hare, E., Hofmann, H., Carriquiry, A. *et al.* Automatic matching of bullet land impressions. *The Annals Appl. Stat.* **11**, 2332–2356, [10.1214/17-AOAS1080](https://doi.org/10.1214/17-AOAS1080) (2017).
- 187
- 188 14. Ju, W. & Hofmann, H. The R Journal: An Open-Source Implementation of the CMPS Algorithm for Assessing Similarity of Bullets. *The R J.* **14**, 267–285, [10.32614/RJ-2022-035](https://doi.org/10.32614/RJ-2022-035) (2022).
- 189
- 190 15. Cleveland, W. S., Grosse, E. & Shyu, W. M. Local Regression Models. In *Statistical Models in S* (Routledge, 1992).
- 190
- 190 16. Hofmann, H., Vanderplas, S., Krishnan, G. & Hare, E. X3ptools: Tools for Working with 3D Surface Measurements, [10.32614/CRAN.package.x3ptools](https://doi.org/10.32614/CRAN.package.x3ptools) (2018).

191 **Acknowledgements**

192 This work was partially funded by the Center for Statistics and Applications in Forensic Evidence (CSAFE) through Cooper-
193 ative Agreement 70NANB20H019 between NIST and Iowa State University, which includes activities carried out at Carnegie
194 Mellon University, Duke University, University of California Irvine, University of Virginia, West Virginia University, Univer-
195 sity of Pennsylvania, Swarthmore College and the University of Nebraska-Lincoln.

196 **Author contributions statement**

197 Let's follow the Elsevier definitions: <https://www.elsevier.com/researcher/author/policies-and-guidelines/credit-author-statement>

198 Y.L.: Methodology, Software, Validation, Data Curation, Writing - Draft; H.H.: Conceptualization, Methodology, Valida-
199 tion, Writing - Review & Editing; C.M.: Lab supervision; E.A.: Physical Specimen, Scanning; J.S: Forensic advice; A.C.:
200 Funding acquisition.

201 All authors reviewed the manuscript.

202 **Competing interests**

203 (mandatory statement)

204 H.H. is a technical advisor to AFTE (Association of Firearms and Toolmarks Examiners), fellow of the ASA (American
205 Statistical Association), and committee member of the ASA Forensic Science Committee. H.H. has testified as court witness
206 on behalf of judge April Neubauer, NY State Supreme Court Criminal Term in New York City. [other competing interests -](#)
207 [Alicia?](#)